ResearchGate

See discussions, stats, and author profiles for this publication at: https://www.researchgate.net/publication/23162422

Structural Properties of Plant and Mammalian Lipoxygenases. Temperature-Dependent Conformational Alterations and Membrane Binding Ability †

ARTICLE *in* BIOCHEMISTRY · OCTOBER 2008

Impact Factor: 3.02 · DOI: 10.1021/bi800638v · Source: PubMed

CITATIONS
19

READS
18

9 AUTHORS, INCLUDING:

Almerinda Di Venere
University of Rome Tor Vergata
48 PUBLICATIONS **480** CITATIONS
SEE PROFILE

Igor Ivanov
University of Rostock
63 PUBLICATIONS **635** CITATIONS
SEE PROFILE

Annalaura Sabatucci
Università degli Studi di Teramo
23 PUBLICATIONS **239** CITATIONS
SEE PROFILE

Enrico Dainese
Università degli Studi di Teramo
53 PUBLICATIONS **744** CITATIONS
SEE PROFILE

Available from: Hartmut Kühn
Retrieved on: 31 January 2016

Structural Properties of Plant and Mammalian Lipoxygenases. Temperature-Dependent Conformational Alterations and Membrane Binding Ability[†]

Giampiero Mei,[‡,§] Almerinda Di Venere,[‡,§] Eleonora Nicolai,[‡,§] Clotilde B. Angelucci,[||] Igor Ivanov,[⊥] Annalaura Sabatucci,[||] Enrico Dainese,[||] Hartmut Kuhn,[⊥] and Mauro Maccarrone*[,‡,||,#]

NAST Centre, Nanoscienze & Nanotecnologie & Strumentazione, 00133 Rome, Italy, Department of Experimental Medicine and Biochemical Sciences, University of Tor Vergata, Via Montpellier 1, 00133 Rome, Italy, Department of Biomedical Sciences, University of Teramo, Piazza Aldo Moro 45, 64100 Teramo, Italy, Institute of Biochemistry, University Medicine Berlin—Charité, Monbijoustrasse 2, 10117 Berlin, Germany, and European Center for Brain Research (CERC)/Santa Lucia Foundation, Via Ardeatina 306, 00197 Rome, Italy

Received April 10, 2008; Revised Manuscript Received July 7, 2008

ABSTRACT: Lipoxygenases form a heterogeneous family of lipid peroxidizing enzymes, which have been implicated in the synthesis of inflammatory mediators, in cell development and in the pathogenesis of various diseases with major health and political relevance (atherosclerosis, osteoporosis). The crystal structures of various lipoxygenase-isoforms have been reported, and X-ray coordinates for enzyme−ligand complexes are also available. Although the 3D-structures of plant and animal lipoxygenase-isoforms are very similar, recent small-angle X-ray scattering data suggested a higher degree of motional flexibility of mammalian isozymes in aqueous solutions. To explore the molecular basis for these differences we performed dynamic fluorescence measurements that allowed us to study temperature-induced conformational changes arising from three-dimensional fluctuations of the protein matrix. For this purpose, we first investigated the impact of elevated temperature on activity, secondary structure, tertiary structure dynamics and conformational alterations. Applying fluorescence resonance energy transfer we also tested the membrane binding properties of the two lipoxygenase-isoforms, and compared their binding parameters. Taken together, our results indicate that the rabbit 12/15-lipoxygenase is more susceptible to temperature-induced structural alterations than the soybean enzyme. Moreover, the rabbit enzyme exhibits a higher degree of conformational flexibility of the entire protein molecule (global flexibility) and offers the possibility of augmented substrate movement at the catalytic center (local flexibility).

Lipoxygenases LOXs[1] form a heterogeneous family of fatty acid dioxygenases that are widely distributed in plants and animals (*1, 2*). Completion of the human genome project revealed that there are six functional LOX genes, which encode for six different human isoenzymes (*3*). The biological activity of most mammalian LOX-isoforms is not completely understood. 5-LOXs are involved in the biosynthesis of inflammatory leukotrienes (*1*), but other isoforms have been implicated in cell death and differentiation (*4*), bone development (*5*), cancer metastasis (*6*) and atherogenesis (*7*).

The structural biology of the LOX family is not well developed. Crystal structures have been reported for plant and nonmammalian LOX-isoforms (*8*−*12*). Unfortunately, for mammalian LOXs X-ray coordinates are only available for the rabbit 12/15-LOX-inhibitor complex (*13*), and on the basis of these data a 3D-model for the human 5-LOX has been worked out (*14*). All LOX-isoforms constitute single polypeptide molecules that are folded into a two-domain structure (*8*−*13*). The large C-terminal domain contains the catalytic non-heme iron that is buried deeply inside the putative substrate-binding pocket. The small N-terminal domain consists of antiparallel β-sheets and is interconnected to the catalytic domain by an unstructured stretch of amino acids. For the soybean LOX-1 (sb-15-LOX) the two subunits share a 2.600 Å^2 interface that constitutes a solvent filled crevice (*9*). Detailed evaluation of the corresponding X-ray coordinates suggested that the overall structures of the two domains are rather stable and that the N-terminal β-barrel domain might move as a stable unit relative to the catalytic domain only by rocking along its surface but not by swinging away from it (*9*). This conclusion is consistent with recent

[†] Financial support for this study was provided by the European Commission (FP6, LSHM-CT-2004-0050333) to H.K. and by grants from Ministero dell'Università e della Ricerca (PRIN 2005 and FIRB 2006 projects), from Fondazione Cassa di Risparmio di Teramo (Tercas, 2004 and 2005), and from Agenzia Spaziale Italiana to M.M. (DCMC and MoMa projects 2006).

* Author to whom correspondence should be addressed: Department of Biomedical Sciences, University of Teramo, Piazza A. Moro 45, I-64100 Teramo, Italy. Tel: +39-0861-266875. Fax: +39-0861-266877. E-mail: mmaccarrone@unite.it.

[‡] NAST Centre, Nanoscienze & Nanotecnologie & Strumentazione.

[§] University of Tor Vergata.

[||] University of Teramo.

[⊥] University Medicine Berlin—Charité.

[#] CERC/Santa Lucia Foundation.

[1] Abbreviations: LOX, lipoxygenase; DPPC, 1,2-dipalmitoyl-*sn*-glycero-3-phosphocholine; POPC, 1-palmitoy-2-oleyl-*sn*-glycero-3-phosphocholine; dansyl-DHPE: *N*-(5-dimethylaminonaphthalene-1-sulfonyl)-1,2-dihexadecanoyl-*sn*-glycero-3-phosphoethanolamine; FRET, fluorescence resonance energy transfer; LUVs, large unilamellar vesicles; Py-PE, 1,2-dioleoyl-*sn*-glycero-3-phosphoethanolamine-*N*-1-pyrenesulfonyl.

10.1021/bi800638v CCC: $40.75 © 2008 American Chemical Society
Published on Web 08/12/2008

investigations into the solution structure of sb-15-LOX, which did not provide any evidence for major linear dislocation of the N-terminal domain (*15*). In contrast, X-ray scattering data on the rabbit reticulocyte 12/15-LOX (rr-12/15-LOX) revealed a high degree of motional flexibility of the enzyme in aqueous solutions, and this conclusion was apparently supported by site-directed mutagenesis and membrane binding studies (*16*). Recent reevaluation of the X-ray coordinates obtained for the rr-12/15-LOX-inhibitor complex (*13*) suggested two different enzyme conformations (*17*). When the inhibitor is bound at the active site, rr-12/15-LOX adopts a closed conformation, in which helix α2 blocks the entrance to the substrate-binding pocket (*17*). In contrast, when the substrate-binding pocket is empty (open form), helix α2 is restructured and its core-unit moves outside by about 12 Å to open the substrate-binding pocket. Interestingly, displacement of this surface helix is paralleled by conformational alterations at the active site. Here helix α18 containing the sequence determinants of the positional specificity I593 (*18*) retreats from the cavity enlarging the volume of the substrate-binding pocket. This movement is also quite substantial, since the α-carbon atoms of I597, the C-terminal amino acid of this helix in both conformers, are separated by almost 6 Å (*17*).

Taken together, these data suggest that rr-12/15-LOX exhibits a high degree of structural flexibility, which appears to be limited for the soybean enzyme. To explore the molecular basis for the different dynamic properties of the two LOX isozymes, we performed dynamic fluorescence measurements that allowed us to study temperature-induced conformational changes arising from three-dimensional fluctuations of the protein matrix. For this purpose, we first investigated the impact of elevated temperatures on activity, secondary structure, tertiary structure dynamics and conformational alterations. Applying fluorescence resonance energy transfer, we also tested the membrane binding properties of the two LOX-isoforms and compared their binding parameters. Our results indicate that the rr-12/15-LOX is more susceptible to temperature-induced structural alterations than sb-15-LOX and exhibits a higher degree of motional flexibility.

MATERIALS AND METHODS

Chemicals. BODIPY-B3824 and BODIPY-B3825 were from Invitrogen (Carlsbad, USA). Linoleic (9, 12-octadecadienoic) acid and buffers were purchased from Sigma Chemical CO (St. Louis, MO).

Preparation of Native LOX-species. The soybean (*Glycine max* [L.] Merrill, Williams) LOX1 (sb-15-LOX) was purified from seeds combining sequential ammonium sulfate precipitation and both cationic and anionic exchange chromatography (CM Sephadex C-50 and DEAE Sephadex A-50, GE-Healthcare Bio-Sciences, Uppsala, Sweden); a further step of purification was added, by using a fast protein liquid chromatography apparatus (FPLC Akta Explorer, GE-Healthcare Bio-Sciences, Uppsala, Sweden). The rabbit 15-LOX was prepared from a stroma-free supernatant of a reticulocyte-rich blood cell suspension by sequential fractionated ammonium sulfate precipitation, hydrophobic interaction chromatography (Biogel SEC Phenyl-5-PW column, Biorad, Munich, Germany) and anion exchange chromatography (Resource-Q column, GE-Healthcare Bio-Sciences, Uppsala, Sweden). All spectroscopic measurements of both sb-15-LOX and rr-12/15-LOX were carried out in Tris HCl, pH = 7.2, 50 mM, at a protein concentration varying in the range ≈5−10 μM.

Activity Assays. The enzymatic activity of the two LOX-isoforms was assayed by the standard spectrophotometric procedure measuring the time-dependent increase in absorbance at 235 nm (formation of conjugated dienes) in a 0.1 M phosphate buffer, pH 7.4. Linoleic acid (in the range 5−500 μM) was employed as substrate.

CD and Absorption Spectroscopy Measurements. The unfolding process was monitored by CD measurements at 220 nm using a Jasco-710 spectropolarimeter at different temperatures (°C), using a 0.1 cm quartz cuvette. The alpha helix and beta structure content was estimated with the Jasco software based on the comparison between the measured spectrum and a linear combination of reference spectra obtained form a set of proteins with known secondary and tertiary structure (*19, 20*). Enzymatic activity (in the presence or in the absence of BODIPY) was assayed spectrophotometrically at 25 °C, by recording the formation of conjugated hydroperoxides from linoleic acid at 234 nm on a Perkin-Elmer Lambda 18 spectrophotometer.

Dynamic Light Scattering Measurements. Light scattering measurements were performed on a Horiba (Kyoto, Japan) LB-500 dynamic light scattering nanoparticle size analyzer, equipped with a 650 nm, 5 mW laser diode. Data analysis was performed using the accompanying software based on a Fourier-transform deconvolution procedure.

Fluorescence Spectroscopy Measurements. Dynamic fluorescence and anisotropy measurements were performed on a K2 spectrofluorometer (ISS, Champaign, IL) equipped with Glan-Thompson polarizers, using the phase-shift and demodulation technique. During all measurements a constant temperature in the sample holder was maintained by an external bath circulator and carefully checked by a thermocouple. Two laser diodes with emission wavelengths at 300 ± 6 nm and 370 ± 6 nm were used as light sources to monitor tryptophan and BODIPY fluorescence. The emission was observed through cutoff filters (WG 320 and WG 420, respectively) to avoid scattered light.

LOX samples were incubated in the presence of BODIPY in a K^+-phosphate buffer 100 mM, at pH = 8.0, 25 °C (BODIPY to protein ratio 60:1) for about 30 min. The BODIPY in excess was then removed by filtration of the solution through a D-salt excellulose plastic desalting column, equilibrated at pH = 7.2. The anisotropy decay of the BODIPY−LOX complexes were fitted according to a double exponential decay function, with two distinct rotational correlation times, ϕ_1 and ϕ_2. The theoretical rotational times for rr-12/15-LOX and rr-12/15-LOX are 40 and 30 ns, using molecular weights of about 95 kDa and 75 kDa, respectively, assuming a spherical and rigid shape for both. Actually, considering that they are more similar to prolate ellipsoids, the longer rotational component (ϕ_2) was considered a first order approximation of the overall tumbling of the dye together with the whole enzyme (*21, 22*).

Membrane Binding. To evaluate the effect of the physical state of the membrane on the protein−lipid interaction, we carried out binding experiments with large unilamellar vesicles (LUV) with two different lipid compositions: 1,2-

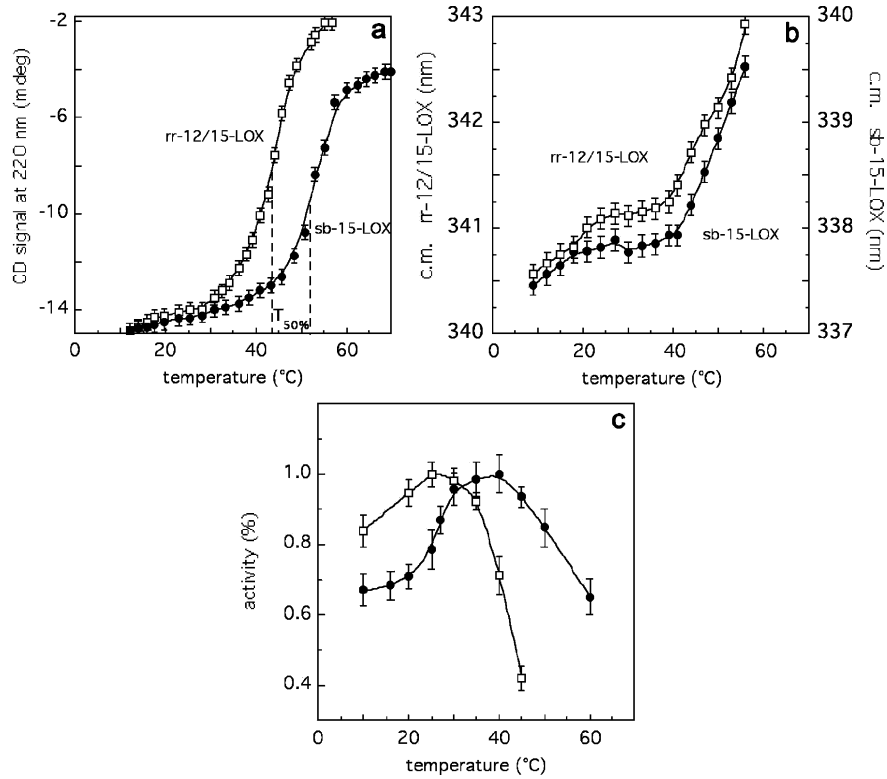

FIGURE 1: Thermal denaturation of LOX-isoforms. Aqueous solutions of sb-15-LOX (filled symbols) and rr-12/15-LOX (empty symbols) were heated to different temperatures, and CD signals at 220 nm were recorded. Panel a: CD-signal intensity. Panel b: center of mass of fluorescence spectrum. Panel c: enzymatic activity.

dipalmitoyl-*sn*-glycero-3-phosphocholine (DPPC), a lipid known to be in the solid-like gel phase (β-phase) at the temperatures used for the binding experiments, and 1-palmitoy-2-oleyl-*sn*-glycero-3-phosphocholine (POPC), an abundant lipid in animal cell membranes that is in the liquid disordered crystalline phase (α-phase, l_c) at the same temperatures (*23, 24*). Interaction of the LOX-isoforms with DPPC and POPC vesicles was performed at 22 and 37 °C in the presence of 0.2 mM Ca^{2+}, using a protein concentration of 0.2 μM in all experiments. Membrane binding data were elaborated through nonlinear regression analysis, using the Sigma Plot 2000 program (Systat Software, London, U.K.).

Fluorescence Resonance Energy Transfer (FRET). FRET was measured on the basis of a decrease in the emission intensity of the energy donor (Trp residues). Since FRET is based on short-range (28 Å for the Trp-pyrene pair) dipole−dipole interactions between energy donors and acceptors, the observed effect indicates binding of protein molecules to vesicles. After correction of the FRET data for sample dilution and for increase of emission intensity upon binding to unlabeled vesicles, binding isotherms were constructed by calculation of the changes in emission intensities of tryptophans at each lipid concentration [L] relative to the zero lipid level, namely ΔF.

$$\Delta F = \Delta F_{max} \frac{[L]}{[L]_{1/2} + [L]} \quad (1)$$

Each curve was used to determine the saturating value of ΔF at high lipid concentration (i.e., ΔF_{max}) and the value of lipid concentration giving the 50% of saturation ($\Delta F = (1/2)\Delta F_{max}$), namely $L_{1/2}$. Then, ΔF_{max} were used to construct the experimental binding isotherms, i.e. the dependence of $\Delta F/\Delta F_{max}$ on [L]. The analysis of these curves was carried out using a binding model, according to which each free protein molecule binds to an unoccupied binding site at the membrane surface, implementing a method described previously (*25, 26*). Nonlinear regression analysis of the different binding isotherms allowed the calculation of the values of dissociation constant K_d and the number of lipid molecules (N) per protein binding site. It can be demonstrated that, at half-saturation of protein binding to membranes, K_d depends only on $[L]_{1/2}$, N, protein concentration [P], and the fraction of lipids accessible for the protein interaction (δ), according to the following equation:

$$K_d = \frac{\delta}{N}[L]_{1/2} - \frac{[P]}{2} \quad (2)$$

The value of the parameter δ for membrane vesicles with an external diameter of 100 nm is ~0.52, as previously reported. (*26*)

RESULTS

Temperature-Dependent Unfolding of Plant and Mammalian LOX-Isoforms. To compare the thermal stability of rr-12/15-LOX and sb-15-LOX we initially tested the temperature dependence (10−70 °C) of enzymatic activity (Figure 1, panel c) and related these changes to alterations in the secondary and tertiary structure (CD and fluorescence measurements, respectively). From Figure 1a it can be seen that the half-transition temperature ($T_{50\%}$) is higher for sb-15-LOX (51 °C vs 43 °C), indicating that the plant enzyme is more thermostable. The shape of the fluorescence curves that is determined by the change in the spectral center of mass suggests that the process is more complex than a simple two-state transition (Figure 1b).

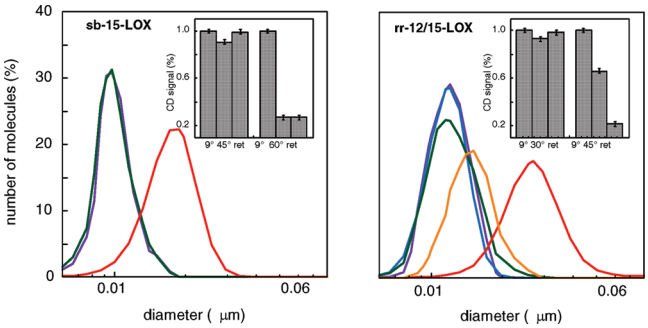

FIGURE 2: Aggregation and reversibility of structural alterations induced by high temperature. Particle size distribution as a function of temperature (10 °C, purple; 30 °C, blue; 45 °C, green; 50 °C, orange; and 60 °C, red lines). In the insets the % CD signal is reported at different temperature values (see text).

Since an increase in temperature frequently induces protein aggregation, we assayed formation of LOX aggregates by light scattering measurements. As indicated in Figure 2, relevant aggregates can be detected for sb-15-LOX at 60 °C while for rr-12/15-LOX the aggregation process is already initiated between 45 and 50 °C. In both cases, the temperature threshold for aggregation is paralleled by a rapid loss in the native tertiary structure of the enzyme (Figure 1b). We therefore investigated to what extent protein aggregation prevents correct structural refolding. For this purpose a solution of sb-15-LOX was heated from 9 to 45 °C and then cooled down to the starting temperature. In a second experiment the solution was heated from 9 to 60 °C and then cooled down to 9 °C. Because of the higher temperature sensitivity of the rr-12/15-LOX, the temperature profile was modified (9 to 30 °C and back to 9 °C; 9 to 45 °C and back to 9 °C). The results of these experiments (Figure 2, insets) indicate that for both enzymes the structural alterations (changes in the CD-spectra) induced by increasing the temperature to 30 °C (rr-12/15-LOX) or 45 °C (sb-15-LOX) were completely reversible. However, heating the enzyme solutions any further (60 °C for sb-15-LOX, 45 °C for rr-12/15-LOX) induced irreversible structural alterations. Similar results were obtained when we assayed the catalytic activity as readout parameter (data not shown), and additional experiments with different temperature profiles (data not shown) suggested that the threshold temperatures (loss of reversibility) were above 45 °C for sb-15-LOX and 35 °C for rr-12/15-LOX.

Analysis of Tertiary Structural Dynamics and Conformational Changes. LOX-isoforms constitute single polypeptide chain proteins, which are folded into a two domain structure (*9, 13*). The large C-terminal domain contains the catalytic non-heme iron, but the N-terminal C2-domain is not essential for catalytic activity for several LOX-isoforms (*27, 28*). To gain insights into protein dynamics, which might involve interdomain movement, we next characterized the temperature-dependent structural alterations by fluorescence lifetime measurements of tryptophans. The fluorescence signal of tryptophan is sensitive to polarity and mobility of the surrounding environment (*29*). Thus, recording temperature-dependent alterations in tryptophan fluorescence allowed us to map the conformational heterogeneity of the protein tertiary structure, that is caused by structural fluctuations in the nanosecond time scale. Previous measurements (*30*) have demonstrated that for a complex molecular system such as sb-15-LOX the fluorescence decay can be fitted according to a bimodal Lorentzian distribution of lifetimes, and these data were confirmed in this study (Figure 3a,b). The short and long components were significantly affected by temperature; the width of the fluorescence signals was increased, and the peak was shifted to shorter lifetime values. The size of the full width at half-maximum, which reflects the degree of heterogeneity, has been plotted against temperature and reported in the inset. As long as the temperature was kept below 40 °C, no major effects were observed. Then, structural heterogeneity increases, reaching a maximum at around 55−60 °C. Such behavior was expected, since at these temperatures multiple enzyme conformers should be present because of partial denaturation (*31*−*34*). Fluorescence dynamics of rr-12/15-LOX resembles that of the soybean enzyme, but again the onset of alterations was shifted to lower temperatures. The widths of the fluorescence signals approached 0.5 ns at 60 °C (Figure 3c,d insets), which is almost the same value obtained for sb-15-LOX at 70 °C (Figure 3a,b, insets). Interestingly, broadening of the fluorescence signals starts around 40 °C, which is close to the threshold temperature for the onset of dysfunction (Figure 1c), unfolding (Figure 1a,b) and irreversibility (Figure 2) of rr-12/15-LOX.

The temperature dependence of the catalytic activity of sb-15-LOX deserves more detailed discussion. From Figure 1c it can be seen that there is hardly any increase in enzymatic activity between 10 and 20 °C, and this result apparently contradicts the Arrhenius equation. It should, however, be stressed that alterations in the reaction temperature may impact both structural dynamics of the enzyme molecule and the physicochemical state of the substrate. These two processes might either synergize or antagonize each other so that the resulting net effect of temperature on catalytic activity might actually be zero.

Motional Flexibility of the Fatty Acids Access Channel. To explore the structural flexibility of the fatty acid binding pocket, we applied fluorescence dynamic anisotropy techniques using BODIPY fatty acids analogues as probes. These fluorescence fatty acids were specifically designed to interact with fatty acid-binding proteins (*35*). Initially, we selected two different probes for these experiments: BODIPY-B3824 (fluorescence label is localized in the middle of the fatty acid chain), and BODIPY-D3825 (fluorescence label is localized closer to the carboxylic group) (*35*). While BODIPY-B3824 was not a competitive LOX-inhibitor, and thus it was not suited for our experiments, BODIPY-D3825 was shown to compete with the substrate fatty acid for binding at the active site of sb-15-LOX and rr-12/15-LOX with a K_i of approximately 9 and 1 μM, respectively (data not shown). Next, we performed fluorescence anisotropy measurements of BODIPY-D3825 bound at the active site of the two LOX-isoforms, as function of increasing temperatures between 10 °C and 40 °C; the experimental data were fitted with two distinct rotational correlation times, ϕ_1 and ϕ_2. The shorter correlation time (ϕ_1), which mirrors probe segmental motion, is strictly related to the environment surrounding the probe. Upon binding at the active site, BODIPY-D3825 provides direct information on the dynamics of amino acid residues located at the catalytic center. Comparing the short rotational correlation times of the two LOX-isoforms (Figure 4) one may conclude that ϕ_1 is much smaller for rr-12/15-LOX.

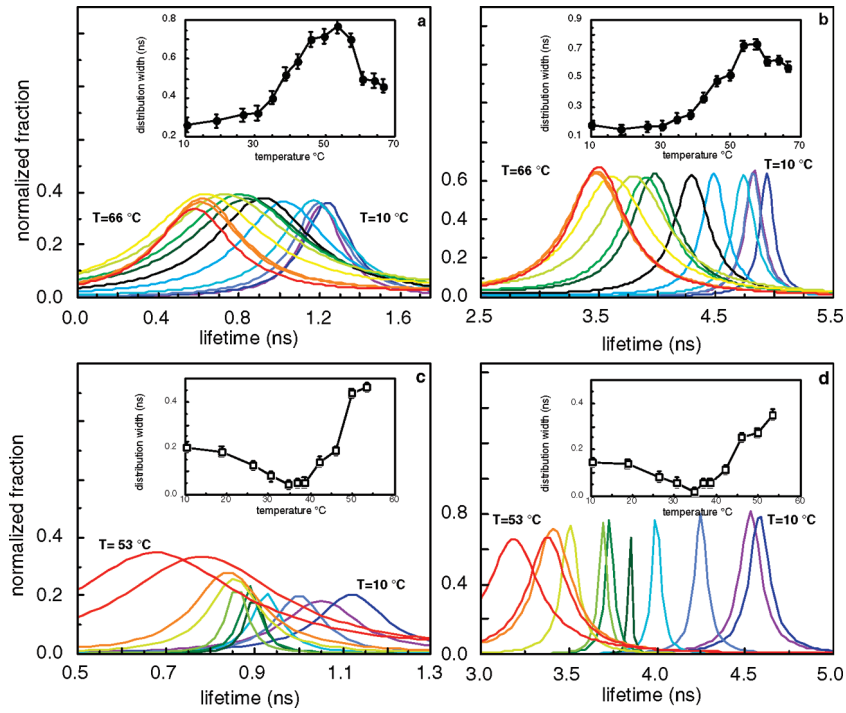

FIGURE 3: Temperature-dependent fluorescence lifetime distributions of LOX isoforms. Upper panels: Fluorescence dynamics of an aqueous solution (≈5−10 μM) of sb-15-LOX were recorded at increasing temperatures in the range of 10 to 66 °C (increasing from the right to the left). For better clarity the short (a) and long (b) lifetime components were plotted separately. In the insets, the values of the full width at half-maximum are shown as a function of temperature. Lower panels: Fluorescence dynamics of an aqueous solution of rr-12/15-LOX were recorded at increasing temperatures in the range of 10 to 53 °C (increasing from the right to the left). For better clarity the short (c) and long (d) lifetime components were plotted separately. In the insets, the values of the full width at half-maximum are shown as a function of temperature.

Moreover, ϕ_1 is strongly temperature-dependent for this enzyme, whereas elevated temperature hardly impacted ϕ_1 for the sb-15-LOX. These data suggest that the probe undergoes a faster rotational motion at the active site of the mammalian enzyme. Assuming that the dye segmental motion can be described as a conic trajectory, the amplitude of the cone, θ, and the rotational diffusion coefficient, D, can be evaluated from the anisotropy decay parameters (*33*). At 25 °C, similar rotational amplitudes were calculated for the movement of BODIPY-D3825 at the active site of the two enzymes (20 °C for sb-15-LOX vs 24 °C for rr-12/15-LOX), while the diffusion coefficients are considerably different (0.01 for sb-15-LOX vs 0.14 ns^{-1} for rr-12/15-LOX). Again, these data are consistent with the idea of a higher motional flexibility of the probe at the active site of the rr-12/15-LOX.

The long rotational correlation times, ϕ_2, were more than 1 order of magnitude larger than the respective ϕ_1-values, and were extremely influenced by temperature (Figure 4). This behavior suggests that ϕ_2 may be related to tumbling of the entire protein molecule. Indeed, a rough estimation of the rotational correlation time for a sphere of about 100 kDa yields ≈42 ns (*22*). The lower ϕ_2-value obtained for rr-12/15 LOX might therefore indicate the presence of an enhanced segmental mobility of the two protein domains.

Membrane Binding Properties of LOX-Isoforms. It has been reported before that both LOX-isoforms are capable of binding to biomembranes in a calcium dependent manner (*25, 36, 37*). To explore the impact of membrane binding on enzyme structure, we investigated by fluorescence resonance energy transfer (FRET) the temperature-dependence of LOX binding to large unilamellar vesicles (LUVs)

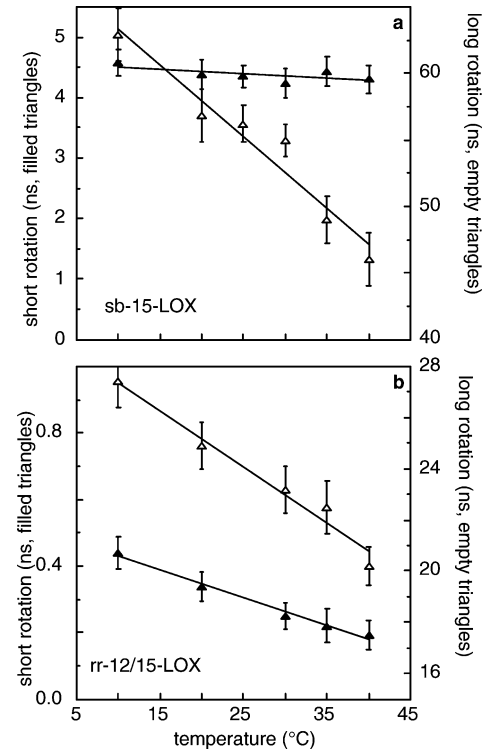

FIGURE 4: Rotational correlation lifetimes of BODIPY-D3825 bound at the active site of LOX-isoforms. LOX-isoforms in aqueous solutions were incubated with BODIPY-D3825, and the rotational correlation lifetimes ϕ_1 (filled symbols) and ϕ_2 (empty symbols) were determined (see Materials and Methods) and plotted vs temperatures. Upper panel: sb-15-LOX. Lower panel: rr-12/15-LOX. In both panels, the solid lines represent the best linear fit of the data.

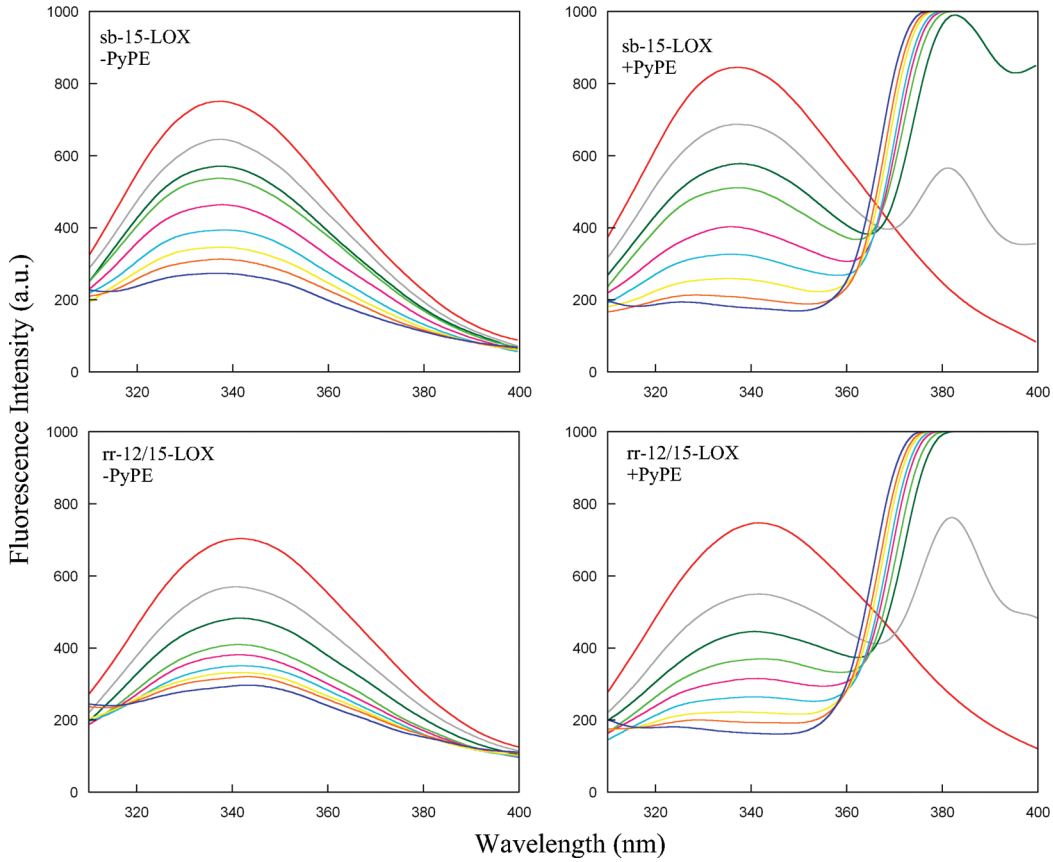

FIGURE 5: Fluorescence emission spectra of membrane bound LOX-isoforms. LOX-isoforms (0.2 μM sb-15-LOX, 0.2 μM rr-12/15-LOX) were incubated at 22 °C with increasing concentrations of POPC vesicles (0−500 μM) containing no or 2 mol % lipophilic Py-PE fluorophor. Upper panel: sb-15-LOX. Lower panel: rr-12/15-LOX. Addition of lipid vesicles causes a decrease in Trp emission intensity as a result of sample dilution. Spectra obtained in the presence of Py-PE show a significant decrease in Trp fluorescence intensity due to resonance energy transfer from Trp of LOXs to Py-PE embedded within the membranes. The change in color from red to blue corresponds to a change in lipid concentration from 0 to 500 μM (concentration steps were made by serial dilutions).

Table 1: Parameters Characterizing the Interaction of LOX-Isoforms with Large Unilamellar Vescicles Composed of DPPC or POPC, in the Presence of 0.2 mM Ca^{2+} at 22°C

lipid	protein	$[L]_{1/2}$ (μM)	K_d (μM)[a]	N[b]	area of interaction (Å^2)
DPPC	sb-15-LOX	73.4 ± 6.9	0.36 ± 0.03	101	6363
DPPC	rr-12/15-LOX	62.8 ± 5.7	0.35 ± 0.03	120	7560
POPC	sb-15-LOX	55.2 ± 4.5	0.35 ± 0.03	43	2790
POPC	rr-12/15-LOX	36.0 ± 2.9	0.28 ± 0.02	44	2772

[a] These values were derived from data shown in Figure 5 and calculated according to eq 2. [b] These values are the mean of at least three different measurements and show a standard error less than 10% ($P < 0.001$).

containing 1,2-dioleoyl-*sn*-glycero-3-phosphoethanolamine-*N*-1-pyrenesulfonyl (Py-PE) as fluorescence probe. Addition of dipalmitoyl-*sn*-glycero-3-phosphocholine (DPPC) lipid vesicles without Py-PE induced a decrease in tryptophan fluorescence as a result of sample dilution (Figure 5, left panels). When we titrated the two LOX-isoforms with Py-PE-containing vesicles (Figure 5, right panels), Trp fluorescence intensity was significantly quenched, because of energy transfer from the tryptophan residues (energy donors) to Py-PE (energy acceptor).

Next, we explored the impact of vesicle composition [DPPC vs 1-palmitoy-2-oleyl-*sn*-glycero-3-phosphocholine (POPC)] vesicles) on binding of the two LOX-isoforms at 22 °C. The values for changes in tryptophan emission intensities at high lipid concentration (ΔF_{max}), calculated for the binding of sb-15-LOX to DPPC and POPC membranes, are comparable to those obtained for rr-12/15-LOX ($\overline{\Delta F_{max}} = 0.85 \pm 0.04$), indicating a similar saturating behavior for the two enzymes. Comparing the half-saturation of binding ($L_{1/2}$) of the two enzymes to DPPC and POCP vesicles, we found that both enzymes preferentially bind to membranes in the liquid disordered phase (POPC vesicles). These data suggest that, despite mammalian and plant LOXs only sharing a low degree of amino acid conservation, they have a convergent three-dimensional structure, which is more suitable to bind lipid bilayers in the liquid disordered phase, a typical feature of biomembranes. Moreover, rather small *N*-values were calculated for the two LOX isoforms upon interaction with POPC vesicles, indicating that the enzymes may interact with a small number of lipid molecules (Table 1). This conclusion was confirmed when we calculated the area of interaction (Table 1). When we compared the membrane binding properties of rr-12/15-LOX with those of the soybean enzyme (Table 1), we found that rr-12/15-LOX exhibits a higher binding affinity and efficiency (K_d

Table 2: Parameters Characterizing the Interaction of sb-15-LOX and rr-12/15-LOX with Large Unilamellar Vesicles Composed of DPPC or POPC, in the Presence of 0.2 mM Ca^{2+} at 37°C

lipid	protein	$[L]_{1/2}$ (μM)	K_d (μM)[a]	N[b]	area of interaction (Å^2)
DPPC	sb-15-LOX	98.5 ± 8.8	0.38 ± 0.03	105	6615
DPPC	rr-12/15-LOX	57.7 ± 5.5	0.18 ± 0.02	109	6867
POPC	sb-15-LOX	61.0 ± 5.7	0.33 ± 0.03	74	4662
POPC	rr-12/15-LOX	36.6 ± 1.0	0.18 ± 0.01	78	4914

[a] These values were obtained from data similar to those reported in Figure 5 and calculated according to eq 2. [b] These values are the mean of at least three different measurements and show a standard error less than 10% ($P < 0.001$).

and $L_{1/2}$) and these differences are particularly prominent for the POPC vesicles.

To explore the impact of temperature on the membrane binding properties of the two LOX-isoforms we repeated these experiments at 37 °C. At this temperature we observed the most relevant conformational and functional differences between the two proteins (Figure 1). The ΔF-values calculated at high lipid concentration for the two LOX-isoforms at 37 °C were comparable ($\overline{\Delta F_{max}} = 0.85 \pm 0.04$). On the other hand, we found that both $L_{1/2}$- and K_d-values for rr-12/15-LOX were smaller than for the soybean enzyme (Table 2). Similar differences were already observed at 22 °C, but they were more pronounced at higher temperatures. Comparing the membrane binding affinity (K_d) of the two enzymes at 22 and 37 °C, we concluded that elevated temperatures hardly affected this property of sb-15-LOX (0.36 vs 0.38 for DPPC, 0.35 vs 0.33 for POPC). In contrast, strongly decreased K_d-values were observed for rr-12/15-LOX at 37 °C (0.35 vs 0.18 for DPPC, 0.28 vs 0.18 for POPC). These data confirm that the soybean enzyme is structurally more stable and its membrane binding properties are hardly affected by temperature alterations. In contrast, rr12/15-LOX is more thermolabile and requires the presence of a lipid environment to be stabilized at higher temperatures.

At 22 °C we found that the number of lipid molecules interacting with one protein particle is higher with DPPC vesicles when compared with POPC liposomes. Similar observations were also made at 37 °C. Although the N numbers did not significantly change between 22 and 37 °C for the DPPC vesicles (101 vs 105 for sb-15-LOX, 120 vs 109 for rr-12/15-LOX), we observed a strong increase in interacting lipids in POPC vesicles for both enzymes (43 vs 74 for sb-15-LOX, 44 vs 78 for rr-12/15-LOX). These data indicate that elevated temperatures induce an increase in interacting lipid molecules in a liquid disordered phase (POPC) but not in DPPC vesicles.

Taking into account (*23, 38*) that the maximum value of the cross-sectional area of a lipid polar head in the case of DPPC and POPC is 68 Å^2, one can estimate the effective area of lipid binding for a single protein molecule (Tables 1 and 2). If the two LOX proteins are considered as prolate ellipsoids of revolution, one can estimate the values of the maximum area available for the membrane binding per protein molecule on the basis of their crystal structures. This area may correspond to half of the surface of the ellipsoid, and was calculated to be 8000 Å^2 for sb-15-LOX and 7100 Å^2 for rr-12/15-LOX. However, under our experimental conditions we determined reduced areas of lipid interactions (Table 2). These data suggest that both proteins preserve a compact structure upon membrane binding and that their surfaces only partly interact with lipid molecules.

DISCUSSION

Different Thermal Denaturation Kinetics of sb-15-LOX and rr-12/15-LOX. Research on the structural biology of LOXs was dominated in the past by X-ray crystallographic studies (*8*−*12*), and application of this static technique led to identification of the putative substrate-binding pocket (*8*−*10*). However, more dynamic approaches of structural elucidation have recently been employed, and the solution structures of both rr12/15-LOX and sb-15-LOX were explored by small-angle X-ray scattering (*15, 16*). These data and molecular dynamics simulations on the rr-12/15-LOX (*39*) suggested that the structural flexibility of LOX-isoforms might vary and that more detailed knowledge on the conformational flexibility of these proteins is required to understand the mechanisms of their catalytic activity at the molecular level. Although dynamic fluorescence cannot compete with X-ray crystallography in terms of structural resolution, it offers the advantage of following the dynamics of structural alterations in aqueous solutions at low protein concentration. Previous unfolding measurements on sb-15-LOX (*40*) suggested that thermal denaturation of the enzyme is initiated in the C-terminal domain, and our results allow similar conclusions for the rr-12/15-LOX.

Dynamic Fluorescence Data Suggest a Higher Motional Flexibility of rr-12/15-LOX. Applying dynamic fluorescence measurements we have previously shown that sb-15-LOX displays a complex fluorescence decay pattern that can be described by a double, continuous distribution of lifetimes (*30*). The rationale for such result resides in the heterogeneous location of the 13 tryptophans in the protein matrix. Furthermore, the width of a continuous distribution of lifetimes may also reflect the number of conformational substates influencing each tryptophan microenvironment during the excited state, providing detailed information on protein dynamics in the nanosecond scale (*29*). In contrast to the data obtained for sb-15-LOX (Figure 3a,b), the behavior of rr-12/15-LOX dynamics in the pre-denaturation range (10−40 °C) was found to be quite different. As a matter of fact, both fluorescence lifetime distributions undergo a progressive and relevant narrowing around their central value (Figure 3c,d). Such an effect is well-known since the appearance of the very first papers about continuous distribution of lifetimes in fluorescence spectroscopy (*41, 42*), and it has been ascribed to faster dynamics. In particular, the increased structural fluctuations induced at higher temperature are expected to enhance the rate of interconversion among different protein conformational substates (*41*). According to this model, the local environment experienced by each tryptophan residue in its excited state becomes more homogeneous and induces a narrowing of the lifetime distribution. Experiments on single tryptophans or on single

tyrosine-containing proteins have not only confirmed this picture, but they have also proven that the effect of temperature is independent of the aromatic probe used (*33, 34*). The rr-12/15-LOX is stable and active only in a narrower temperature range (Figure 1), and therefore the effect on the widths might appear less spectacular than for other proteins (Figure 3c,d). Repeating the lifetime measurements in the presence of glycerol (data not shown) demonstrated that impairment of domain mobility for rr-12/15-LOX reduced the impact of temperature. In fact, the presence of glycerol makes the interconversion among conformational substates more difficult, preventing shrinkage of the lifetime distribution. This effect may be achieved by preferential solvation, a molecular mechanism that forces proteins in glycerol solutions to adopt a compact conformation (*43, 44*). This mechanism slows down the interconversion rate among conformational substates increasing the heterogeneity of the fluorescence decay. As negative control, lifetime measurements of sb-15-LOX in the presence of glycerol showed an extensive broadening effect (data not shown). Taken together, these data suggest that in the pre-denaturation period the overall conformational dynamics in rr-12/15-LOX solution appears to be much faster.

Membrane Binding Properties of sb-15-LOX and rr-12/15-LOX. LOX-isoforms are known to exhibit membrane binding activities, and previous findings indicated that increased intracellular calcium levels induce membrane binding of various LOX isoforms (*30, 36, 37*). It is well-known that membrane binding strongly enhances the catalytic activity of rr-12/15-LOX, but the underlying mechanisms remain elusive (*45*). Our membrane binding data indicated that the LOX structure is stabilized by the interaction with lipid bilayers and that the protein remains properly folded. In contrast to the soybean enzyme, rr-12/15-LOX undergoes augmented structural fluctuations at higher temperatures, that seem to be the structural basis for the more efficient membrane binding. In summary, these results suggested that mammalian LOXs at $T \geq 35$ °C need to be stabilized by membrane binding, while plant enzymes resist elevated temperatures, without requiring membrane interaction. This finding is consistent with previous results obtained *in vivo* with plants exposed to temperature stress (*46*).

Biological Importance of Structural Flexibility. The biology behind the structural differences between plant and mammalian LOXs remains an open question. It may be tempting to speculate that the high degree of motional flexibility of the rr-12/15-LOX offers the evolutionary advantage of more precise regulation of the catalytic activity *via* interdomain interactions, allowing better adjustment of substrate acquisition and chemical processing. In fact, our data on rotational correlation times (Figure 4) obtained by anisotropy measurements provided direct evidence of a higher motional flexibility at the active site of rr-12/15-LOX, and these findings are consistent with the concerted structural rearrangements recently suggested for rr-12/15-LOX upon ligand binding (*17*). The price to be paid for this evolutionary advantage is the less compact 3D-structure that is paralleled by impaired enzyme stability. To compensate for this disadvantage in living cells, the rr-12/15-LOX may interact with lipid bilayers, which apparently stabilize the protein structure. Whether similar high degrees of motional flexibility can also be found for other mammalian LOX-isoforms deserves further investigation. Unfortunately, no direct structural data are currently available for these isoforms, and enzyme supply is also limited. However, high-pressure techniques may be a promising tool to provide further insights into the mechanistic basis of structure-to-function relationships of plant and animal lipoxygenase isoforms.

It has frequently been suggested for homologous enzymes that the catalytic efficiency increases with the degree of motional flexibility. However, for the two LOX-isoforms compared in this study we did not confirm this hypothesis. Although the K_M-values for fatty acid substrates are comparable (*47*), the sb-15-LOX is catalytically more active (k_{cat} of 300 s^{-1} for sb-15-LOX vs 20 s^{-1} for rr-12/15-LOX). The molecular basis for this difference has not yet been clarified, but it might be related to the higher degree of motional flexibility of substrates at the active site, which counteracts precise positioning of the fatty acid molecule in relation to the non-heme iron. Such less precise substrate alignment may hinder catalysis of hydrogen abstraction from a bisallylic methylene, which is the rate-limiting step of the LOX reaction.

ACKNOWLEDGMENT

The technical assistance of Ms. P. C. Gerth (rabbit 12/15-LOX preparation) is greatly acknowledged.

REFERENCES

1. Brash, A. R. (1999) Lipoxygenases: occurrence, functions, catalysis, and acquisition of substrate. *J. Biol. Chem. 274*, 23679–23482.
2. Feussner, I., and Wasternack, K. (2002) The lipoxygenase pathway. *Annu. Rev. Plant Biol. 53*, 275–297.
3. Funk, C. D., Chen, X. S., Johnson, E. N., and Zhao, L. (2002) Lipoxygenase genes and their targeted disruption. *Prostaglandins Other Lipid Mediators 68−69*, 303–312.
4. Maccarrone, M., Melino, G., and Finazzi Agrò, A. (2001) Lipoxygenases and their involvement in programmed cell death. *Cell Death Differ. 8*, 776–784.
5. Klein, R. F., Allard, J., Avnur, Z., Nikolcheva, T., Rotstein, D., Carlos, A. S., Shea, M., Waters, R. V., Belknap, J. K., Peltz, G., and Orwoll, E. S. (2004) Regulation of bone mass in mice by the lipoxygenase gene Alox15. *Science 303*, 229–232.
6. Pidgeon, G. P., Lysaght, J., Krishnamoorthy, S., Reynolds, J. V., O'Byrne, K., Nie, D., and Honn, K. V. (2007) Lipoxygenase metabolism: roles in tumor progression and survival. *Cancer Metastasis Rev. 26*, 503–524.
7. Kuhn, H., Römisch, I., and Belkner, J. (2005) The role of lipoxygenase isoforms in atherogenesis. *Mol. Nutr. Food Res. 49*, 1014–1029.
8. Boyington, J. C., Gaffney, B. J., and Amzel, L. M. (1993) The three-dimensional structure of an arachidonic acid 15-lipoxygenase. *Science 260*, 1482–1486.
9. Minor, W., Steczko, J., Stec, B., Otwinowski, Z., Bolin, J. T., Walter, R., and Axelrod, B. (1996) Crystal structure of soybean lipoxygenase L-1 at 1.4 Å resolution. *Biochemistry 35*, 10687–10701.
10. Pham, C., Jankun, J., Skrzypczak-Jankun, E., Flowers, R. A., and Funk, M. O. (1998) Structural and thermochemical characterization of lipoxygenase-catechol complexes. *Biochemistry 37*, 17952–17957.
11. Skrzypczak-Jankun, E., Bross, R. A., Carroll, R. T., Dunham, W. R., and Funk, M. O. (2001) Three-dimensional structure of a purple lipoxygenase. *J. Am. Chem. Soc. 123*, 10814–10820.
12. Oldham, M. L., Brash, A. R., and Newcomer, M. E. (2005) Insights from the X-ray crystal structure of coral 8R-lipoxygenase: calcium activation via a C2-like domain and a structural basis of product chirality. *J. Biol. Chem. 280*, 39545–39552.
13. Gillmor, S. A., Villasenor, A., Fletterick, R., Sigal, E., and Browner, M. F. (1997) The structure of mammalian 15-lipoxygenase reveals similarity to the lipases and the determinants of substrate specificity. *Nat. Struct. Biol. 4*, 1003–1009.

14. Du, L., Zhang, Z., Luo, X., Chen, K., Shen, X., and Jiang, H. (2006) Binding investigation of human 5-lipoxygenase with its inhibitors by SPR technology correlating with molecular docking simulation. *J. Biochem. 139*, 715–723.
15. Dainese, E., Sabatucci, A., van Zadelhoff, G., Angelucci, C. B., Vachette, P., Veldink, G. A., Finazzi Agrò, A., and Maccarrone, M. (2005) Structural stability of soybean lipoxygenase-1 in solution as probed by small angle X-ray scattering. *J. Mol. Biol. 349*, 143–152.
16. Hammel, M., Walther, M., Prassl, R., and Kuhn, H. (2004) Structural flexibility of the N-terminal beta-barrel domain of 15-lipoxygenase-1 probed by small angle X-ray scattering. Functional consequences for activity regulation and membrane binding. *J. Mol. Biol. 343*, 917–929.
17. Choi, J., Chon, J. K., Kim, S., and Shin, W. (2008) Conformational flexibility in mammalian 15S-lipoxygenase: Reinterpretation of the crystallographic data. *Proteins: Struct., Funct., Bioinf. 70*, 1023–1032.
18. Borngräber, S., Browner, M., Gillmor, S., Gerth, C., Anton, M., Fletterick, R., and Kühn, H. (1999) Shape and specificity in mammalian 15-lipoxygenase active site. The functional interplay of sequence determinants for the reaction specificity. *J. Biol. Chem. 274*, 37345–37350.
19. Yang, J. T., Wu, C. S., and Martinez, H. M. (1986) Calculation of protein conformation from circular dichroism. *Methods Enzym. 130*, 208–269.
20. Venyaminov, S. Y., Baikalov, I. A., Shen, Z. M., Wu, C. S., and Yang, J. T. (1993) Circular dichroic analysis of denatured proteins: inclusion of denatured proteins in the reference set. *Anal. Biochem. 214*, 17–24.
21. Haugland, R. P. (2005) in *The Handbook—a guide to fluorescence probes and labeling technologies*, Molecular Probes, Invitrogen, Eugene, OR.
22. Cantor, C. R., Schimmel, P. R. (1980) *Biophysical chemistry*, Vol. II, W. H. Freeman and Company, San Francisco.
23. Nagle, J. F., and Tristram-Nagle, S. (2000) Structure of lipid bilayers. *Biochim. Biophys. Acta 1469*, 159–195.
24. Litman, B. J., Lewis, E. N., and Levin, I. W. (1991) Packing characteristics of highly unsaturated bilayer lipids: Raman spectroscopic studies of multilamellar phosphatidylcholine dispersions. *Biochemistry 30*, 313–319.
25. Tatulian, S. A., Steczko, J., and Minor, W. (1998) Uncovering a calcium-regulated membrane-binding mechanism for soybean lipoxygenase-1. *Biochemistry 37*, 15481–15490.
26. Pande, A. H., Qin, S., and Tatulian, S. A. (2005) Membrane fluidity is a key modulator of membrane binding, insertion, and activity of 5-lipoxygenase. *Biophys. J. 88*, 4084–4094.
27. Maccarrone, M., Salucci, M. L., van Zadelhoff, G., Malatesta, F., Veldink, G., Vliegenthart, J. F. G., and Finazzi Agrò, A. (2001) Tryptic digestion of soybean lipoxygenase-1 generates a 60 kDa fragment with improved activity and membrane binding ability. *Biochemistry 40*, 6819–6827.
28. Walther, M., Anton, M., Wiedmann, M., Fletterick, R., and Kühn, H. (2002) The N-terminal domain of the reticulocyte-type 15-lipoxygenase is not essential for enzymatic activity but contains determinants for membrane binding. *J. Biol. Chem. 277*, 27360–27366.
29. Lakowicz, J. R. (1999) *Principles of fluorescence spectroscopy*, 2nd ed., Kluwer Academic/Plenum Publishers, New York.
30. Di Venere, A., Salucci, M. L., van Zadelhoff, G., Veldink, G., Mei, G., Rosato, N., Finazzi Agro', A., and Maccarrone, M. (2003) Structure-to-function relationship of mini-lipoxygenase, a 60 kDa fragment of soybean lipoxygenase-1 with lower stability but higher enzymatic activity. *J. Biol. Chem. 278*, 18281–18288.
31. Bismuto, E., Gratton, E., and Irace, G. (1988) Effect of unfolding on the tryptophanyl fluorescence lifetime distribution in apomyoglobin. *Biochemistry 27*, 2132–2136.
32. Mei, G., Rosato, N., Silva, N., Rusch, R., Gratton, E., Savini, I., and Finazzi Agrò, A. (1992) Denaturation of human Cu/Zn Superoxide Dismutase by Guanidine Hydrochloride a dynamic fluorescence study. *Biochemistry 31*, 7224–7230.
33. Silva, N., Jr., Gratton, E., Mei, G., Rosato, N., Rusch, R., and Finazzi-Agrò, A. (1993) Molten globule monomers in human superoxide dismutase. *Biophys.Chem. 48*, 171–182.
34. Ferreira, S. T., Stella, L., and Gratton, E. (1994) Conformational dynamics of bovine Cu, Zn superoxide dismutase revealed by time-resolved fluorescence spectroscopy of the single tyrosine residue. *Biophys. J. 66*, 1185–1196.
35. Thumser, A. E., and Storch, J. (2007) Characterization of a BODIPY-labeled fluorescent fatty acid analogue. Binding to fatty acid-binding proteins, intracellular localization, and metabolism. *Mol. Cell. Biochem. 299*, 67–73.
36. Baba, A., Sakuma, S., Okamoto, H., Inoue, T., and Iwata, H. (1989) Calcium induces membrane translocation of 12-lipoxygenase in rat platelets. *J. Biol. Chem. 264*, 15790–15795.
37. Watson, A., and Doherty, F. J. (1994) Calcium promotes membrane association of reticulocyte 15-lipoxygenase. *Biochem. J. 298*, 377–383.
38. Stillwell, W., and Wassall, S. R. (2003) Docosahexaenoic acid: membrane properties of a unique fatty acid. *Chem. Phys. Lipids. 126*, 1–27.
39. Saam, J., Ivanov, I., Walther, M., Holzhütter, H. G., and Kühn, H. (2007) Molecular dioxygen enters the active site of 12/15-lipoxygenase via dynamic oxygen access channels. *Proc. Natl. Acad. Sci. U.S.A. 104*, 13319–13324.
40. Sudharshan, E., and Appu Rao, A. G. (1999) Involvement of cysteine residues and domain interactions in the reversible unfolding of lipoxygenase-1. *J. Biol. Chem. 274*, 35351–35358.
41. Alcala, J. R., Gratton, E., and Prendergast, F. G. (1987) Interpretation of fluorescence decays in proteins using continuous lifetime distributions. *Biophys. J. 51*, 925–936.
42. Lakowicz, J. R., Cherek, H., Gryczynski, I., Joshi, N., and Johnson, M. L. (1987) Analysis of fluorescence decay kinetics measured in the frequency domain using distributions of decay times. *Biophys. Chem. 28*, 35–50.
43. Gekko, K., and Timasheff, S. N. (1981) Mechanism of protein stabilization by glycerol: preferential hydration in glycerol-water mixtures. *Biochemistry 20*, 4667–4676.
44. Timasheff, D. N. (1993) The control of protein stability and association by weak interactions with water: how do solvents affect these processes? *Annu. Rev. Biophys. Biomol. Struct. 22*, 67–97.
45. Lankin, V. Z., Kuhn, H., Hiebsch, C., Schewe, T., Rapoport, S. M., Tikhaze, A. K., and Gordeeva, N. T. (1985) On the nature of the stimulation of the lipoxygenase from rabbit reticulocytes by biological membranes. *Biomed. Biochim. Acta. 44*, 655–664.
46. Ali, M. B., Hahn, E. J., and Paek, K. Y. (2005) Effects of temperature on oxidative stress defense systems, lipid peroxidation and lipoxygenase activity in Phalaenopsis. *Plant. Physiol. Biochem. 43*, 213–223.
47. Ludwig, P., Holzhutter, H. G., Colosimo, A., Silvestrini, M. C., Schewe, T., and Rapoport, S. M. (1987) A kinetic model for lipoxygenases based on experimental data with the lipoxygenase of reticulocytes. *Eur. J. Biochem. 168*, 325–337.

BI800638V